

RESEARCH

Open Access



Real-time morphological and dosimetric adaptation in nasopharyngeal carcinoma radiotherapy: insights from autosegmented fractional fan-beam CT

Xiao-li Yu^{1,2†}, Jiang Hu^{1†}, Yu-xian Yang^{1†}, Guang-yu Wang¹, Xin Yang¹, Wen-chao Diao¹, Lu Liu¹, Xiao-bo Jiang¹, Chen-di Xu¹, Liu-wen Lin¹, Le-cheng Jia³, Hua Li³, Yan-fei Liu³, Ying Sun^{1*} and Guan-qun Zhou^{1*}

Abstract

Background To quantify morphological and dosimetric variations in nasopharyngeal carcinoma (NPC) radiotherapy via autosegmented fan-beam computed tomography (FBCT) and to inform decision-making regarding appropriate objectives and optimal timing for adaptive radiotherapy (ART).

Methods This retrospective study analyzed 23 NPC patients (681 FBCT scans) treated at Sun Yat-sen Cancer Center from August 2022 to May 2024. The inclusion criterion was as follows: ≥ 1 weekly FBCT via a CT-linac with ≤ 2 fractions between scans. Four deep learning-based autosegmentation models were developed to assess weekly volume, Dice similarity coefficient (DSC), and dose variations in organs at risk (OARs) and target volumes.

Results A systematic review of autosegmentation on FBCT scans demonstrated satisfactory accuracy overall, and missegmentation was manually modified. Linear decreases in volume and/or DSC were observed in the parotid glands, submandibular glands, thyroid, spinal cord, and target volumes ($R^2 > 0.7$). The linear dose variation included coverage of the low risk planning target volume (-3.01%), the mean dose to the parotid glands (+2.45 Gy) and thyroid (+1.18 Gy), the D1% of the brainstem (+0.56 Gy), and the maximum dose to the spinal cord (+1.12 Gy). The greatest reduction in target volume coverage was noted in PGTvns, reaching 7.15%. The most significant dose changes occurred during weeks 3–6.

Conclusions During NPC radiotherapy, the progressive dose deviations may not be corrected through repositioning alone, necessitating ART intervention. As dose variations in OARs rarely exceed 3 Gy and target coverage fluctuations remain within 10%, ART does not need to be performed frequently, and weeks 3–6 represent the most appropriate window.

[†]Xiao-li Yu, Jiang Hu and Yu-xian Yang contributed equally to this work.

*Correspondence:

Ying Sun
sunying@sysucc.org.cn
Guan-qun Zhou
zhougq@sysucc.org.cn

Full list of author information is available at the end of the article



© The Author(s) 2025. **Open Access** This article is licensed under a Creative Commons Attribution-NonCommercial-NoDerivatives 4.0 International License, which permits any non-commercial use, sharing, distribution and reproduction in any medium or format, as long as you give appropriate credit to the original author(s) and the source, provide a link to the Creative Commons licence, and indicate if you modified the licensed material. You do not have permission under this licence to share adapted material derived from this article or parts of it. The images or other third party material in this article are included in the article's Creative Commons licence, unless indicated otherwise in a credit line to the material. If material is not included in the article's Creative Commons licence and your intended use is not permitted by statutory regulation or exceeds the permitted use, you will need to obtain permission directly from the copyright holder. To view a copy of this licence, visit <http://creativecommons.org/licenses/by-nc-nd/4.0/>.

Keywords Morphology, Dosimetry, Autosegmentation, Fan-beam CT, Adaptive radiotherapy, Nasopharyngeal carcinoma

Background

Intensity-modulated radiation therapy (IMRT) is the primary curative approach for nonmetastatic nasopharyngeal carcinoma (NPC). During radiotherapy, tumor regression and patient weight loss often lead to significant changes in the morphology and dosimetry of both the tumor and the organs at risk (OARs) [1–5]. These changes cannot be fully addressed by daily imaging-guided radiotherapy (IGRT) alone. Consequently, adaptive radiotherapy (ART) has emerged as a critical strategy to address these dynamic alterations [6–9].

However, the criteria for implementing ART in head and neck tumors, including NPC, remain poorly defined. Most studies reference factors such as changes in patient weight loss, volume of the parotid glands or target volumes [10–13], but volume changes alone may not fully capture spatial displacement. The Dice similarity coefficient (DSC), which quantifies the spatial overlap between two datasets, offers a more comprehensive assessment of morphological changes in target volumes and OARs.

Furthermore, while the parotid glands and gross tumor volumes (GTVs) were frequently studied, other OARs and target volumes were rarely mentioned [1, 2]. The morphological and dosimetric changes in these structures during radiotherapy remain poorly understood. Insufficient target volume coverage or excessive doses to OARs can compromise tumor control rates or lead to severe radiotherapy-related complications, potentially posing life-threatening risks [2, 14–15]. For example, Belshaw L et al. reported that some head and neck cancer patients experienced a 7.0–7.2 Gy increase in the spinal cord D0.1 cc (Dx% or Dy cc refers to the minimum dose received by the “hottest” x% or y cm³ of the organ) during radiotherapy [16], significantly increasing the risk of radiation-induced spinal cord injury.

To address these challenges, this study retrospectively analyzed NPC patients who received weekly fan beam computed tomography (FBCT) scans during radiotherapy. The target volumes and OARs delineated on FBCT were compared to evaluate weekly changes in volume, DSC, and dose distribution. These findings provided valuable insights for optimizing ART decision-making in NPC treatment.

Methods

Patient

The clinical and radiological data of NPC patients treated with a CT linear accelerator (uRT-linac 506c, Shanghai United Imaging Healthcare Co., Ltd. (UIH), Shanghai, China) at Sun Yat-sen Cancer Center between August

2022 and May 2024 were retrospectively collected. All patients underwent CT simulation and radiotherapy via an integrated “all-in-one” radiotherapy platform, which consolidated simulation, AI-driven autocontouring and treatment planning, quality assurance, and delivery into a unified workflow [17].

The inclusion criteria were as follows: (1) stage I–IVa NPC classified by the 8th edition of the American Joint Committee on Cancer staging system; (2) 18–65 years old, with a Karnofsky performance scale score ≥ 70 ; (3) definitive treatment with IMRT; (4) no previous surgery or radiotherapy for the head and neck region; (5) complete clinical data available; and (6) at least one FBCT scan performed weekly during the treatment period, with ≤ 2 radiotherapy fractions between scans. The exclusion criteria were as follows: (1) incomplete clinical data or treatment and (2) allergies to iodinated contrast agents.

Treatment planning and recalculation on fractional FBCTs

The target volumes and OARs were initially segmented via an AI-based autocontouring system, followed by manual refinement by board-certified radiation oncologists with > 10 years of NPC specialization. Planning target volumes (PTVs) were generated by applying a 3 mm isotropic margin to the GTVs and CTVs. Dose prescriptions followed institutional protocols: PGTVP (primary tumor): 70 Gy in 33 fractions; PGTVN (nodal disease): 66–70 Gy; PCTV1 (high-risk CTV): 60 Gy; PCTV2 (prophylactic CTV): 54 Gy.

Rigid registration between the planning CT and fractional FBCTs was performed. Four 3D U-Net AI models were deployed to autosegment GTVs, CTVs, and OARs on each FBCT. All AI-generated contours were subjected to physician verification and adjustment if needed. The original treatment plan was then recalculated for each FBCT. This workflow enabled longitudinal tracking of volume changes, DSC between planning CT and FBCT contours, and real-time dosimetric delivery for target volumes and OARs.

Autosegmentation of GTVs

Delineation of GTVP boundaries on noncontrast CT is challenging due to soft tissue resolution limitations. To address this, a dual-channel 3D U-Net model was implemented (Fig. 1a). Channel 1 received the FBCT image, whereas Channel 2 incorporated the rigidly registered GTVP contour from the original planning CT. This approach leverages prior spatial information to guide segmentation, achieving a DSC exceeding 0.91 in

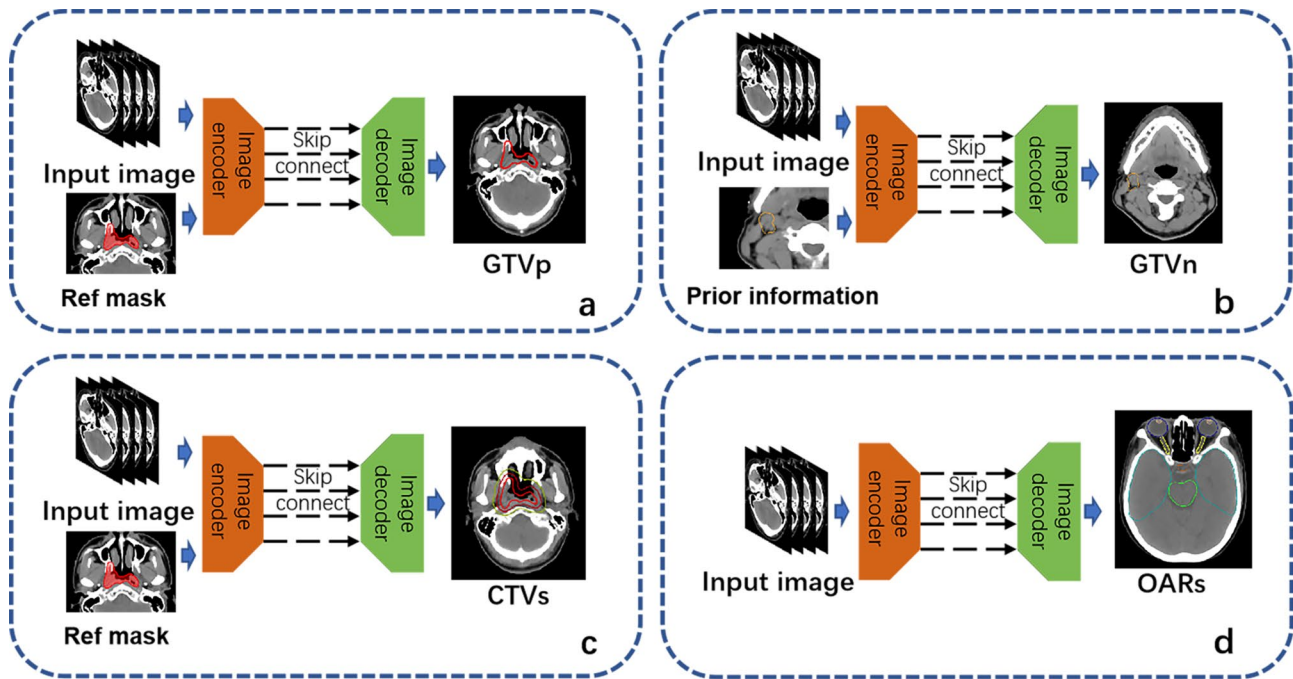


Fig. 1 Networks of autosegmentation for GTVp (a), GTVn (b), CTVs (c) and OARs (d)

the testing cohort, demonstrating high concordance with physician-drawn contours.

For lymph node delineation, two strategies were combined to improve accuracy (Fig. 1b). The first was prior spatial guidance: the GTVn contour from the planning CT was rigidly registered and mapped onto fractional FBCTs to provide an anatomical reference. The second was contextual learning: the model was trained to simultaneously predict GTVn and CTV2, enabling it to learn spatial relationships between them. This dual-task framework achieved a DSC of over 0.71.

Autosegmentation of CTVs

A prior knowledge-guided 3D U-Net architecture was developed for the delineation of CTVs (Fig. 1c). Constraint 1 was the expansion rule: CTV1 was generated by 5–10 mm isotropic expansion from GTVp. By convolving the GTVp mask with the image, a tumor-centric feature map was derived that served as the basis for the model to extract and learn multidimensional features. CTV2 was created by extending 5–10 mm beyond CTV1 and covered the cervical lymphatic drainage regions. Constraint 2 describes the spatial relationships. Specifically, (1) CTV1 was required to encompass GTVp, and CTV2 was required to encompass CTV1 and GTVn. (2) CTV1 avoided the brainstem and temporal lobes; CTV2 additionally spared the parotid glands, submandibular glands, and thyroid unless invaded. Empirical constraints were introduced by sequentially labeling CTV1, CTV2, and OARs with distinct numerical identifiers. In the testing

cohort, the average DSCs for CTV1 and CTV2 were 0.92 and 0.87, respectively.

Autosegmentation of OARs

We developed a multitarget OAR delineation strategy (Fig. 1d) to address the challenges posed by the complex nasopharyngeal anatomy and diverse window width and level requirements for 35 OARs. This system categorized OARs into five anatomically related groups (Supplementary Table 1), enabling efficient spatially consistent contouring within 70 s while maintaining precision. To optimize small OAR segmentation (e.g., lenses, chiasm), we implemented a volume-adaptive dual-path model, which has been detailed in prior study, achieving an average DSC of >0.85 across all structures, with >0.9 for large OARs and >0.75 for small-volume structures [18].

Loss function

The contour loss function was used to enhance the ability of the network to extract pertinent information from the prediction contours. It includes Dice loss and cross-entropy loss.

The Dice loss and cross-entropy loss were calculated as follows:

$$L_{\text{dice}} = -\frac{2}{C} \sum_{k \in C} \frac{\sum_{i \in N} G(a)_k^i P(a)_k^i}{\sum_{i \in N} G(a)_k^i + \sum_{i \in N} P(a)_k^i} \quad (1)$$

$$L_{CE} = 1 - \frac{1}{N} \sum_{i \in N} \sum_{k \in C} G_i^k \log(P_i^k) \quad (2)$$

where G denotes the GT and P was Pred.

The objective loss L was the weighted sum of the Dice loss L_{dice} and cross-entropy L_{CE} .

$$L = \alpha_1 L_{dice} + \alpha_2 L_{CE} \quad (3)$$

The coefficient weights α_1 and α_2 were empirically set to 0.5 and 0.5, respectively. A grid search was conducted to determine the values of the coefficients.

Changes in volume, DSC and dose

The volume, DSC [$DSC = 2 \times |A \cap B| / (|A| + |B|)$] and dosimetric parameters for target volumes and OARs were systematically evaluated across treatment weeks 1–7. Weekly metrics were derived from FBCT scans, with week 1 data extracted from fractions 1–3 and subsequent weeks sampled at 5-fraction intervals. If no FBCT was

available for a scheduled interval, the mean of adjacent fractions was used; if only one neighboring scan existed, its value was adopted.

For each structure, the average volume over weeks 1–7 was calculated and defined as Vmean. Weekly volumes were recorded as $V_{week_1...7}$. The percentage volumetric difference of each week was calculated via the following formula: $[(V_{week_x} - V_{mean}) / V_{mean}] \times 100\%$ ($x = 1, 2, 3... 7$). To account for delineation and positioning errors, if the percentage differences of each week were <2.5%, the structure was considered volume constant. Otherwise, a linear fit was applied to assess the trend over time. This same approach was also applied to analyze changes in the DSC.

The dose distributions were recalculated for each FBCT via the original treatment plan. The dosimetric parameters for each structure were derived from a questionnaire survey conducted by 20 experts with >5 years of NPC specialization, with the highest number of votes being selected; the specific parameters were shown in Supplementary Table 2. The V100% (percentage coverage of 100% of the prescription dose) was selected for PGTVp and PGTVns; the V95% for PTV1 and PTV2; the D1% for the brainstem and temporallobes; the maximum dose (Dmax) for the spinal cord, optic nerves, chiasm, and temporomandibular joints (TMJs); and the D0.03 cc for the mandibles. Dmean was used for the eyes, lenses, parotid glands, submandibular glands, oral cavity, thyroid, pituitary, bony part of eustachian tubes (ETs), cochleas, internal auditory canals (IACs), larynx_supraglottic, larynx_glottis, tympanic cavities, and vestibul semises. Linear fitting was then performed.

Table 1 Patients' characteristics

	Patients (total)	
	n	%
Sex		
Male	19	82.61
Female	4	17.39
Age (years)	49 (23–69)	
T staging (AJCC 8 th)*		
T1	0	0
T2	1	4.34
T3	19	82.61
T4	3	13.04
N staging (AJCC 8 th)*		
N0	6	26.09
N1	9	39.13
N2	6	26.09
N3	2	8.70
Overall staging (AJCC 8 th)*		
I	0	0
II	0	0
III	18	78.26
IV	5	21.74
Neoadjuvant Chemotherapy		
Yes	11	47.83
No	12	52.17
Concurrent Chemotherapy		
Yes	21	91.30
No	2	8.70
Number of FBCT scans	32 (18–33)	
Body surface area (m ²)	1.82 (1.36~2.04)	
Body mass index	25.21 (19.21~28.44)	

Abbreviations: FBCT=Fan Beam Computed Tomography; AJCC=American Joint Committee on Cancer

* The 8th edition of the American Joint Committee on Cancer staging system

Statistics

Origin 8 (Massachusetts, United States) was used to perform linear fitting of the volume, DSC and dosimetric parameters of the target volumes and OARs. A coefficient of determination (R^2) ≥ 0.7 was considered indicative of a good linear fit.

Results

Patients

A total of 23 patients were enrolled, yielding 681 FBCT scans. The number of FBCT scans per patient ranged from 18 to 33. Specifically, 5 patients had fewer than 25 scans, while 18 patients had more than 30 scans, including 10 patients with exactly 33 scans. The clinical characteristics of all patients were summarized in Table 1.

Assessment of autosegmentation accuracy

A systematic review of autosegmentation on FBCT scans demonstrated satisfactory delineation accuracy overall. However, manual corrections were required for certain structures exhibiting suboptimal autocontouring.

Specifically, one FBCT scan showed incomplete delineation of the GTVp and the oral cavity; three FBCT scans from two patients exhibited an incomplete brainstem; and five FBCT scans from three patients had underestimated spinal cord contours. In addition, multiple FBCT scans revealed suboptimal contours for the chiasm, pituitary, cochlea, and vestibul semis. All remaining target volumes and OARs maintained clinically acceptable autocontours without adjustments.

Volume and DSC changes

The parotid glands, submandibular glands, thyroid, and all target volumes exhibited absolute percentage volume differences exceeding 2.5%. Linear fitting analysis revealed a gradual decrease in the parotid glands, submandibular glands, thyroid, and all target volumes, with $R^2 > 0.7$ (Fig. 2a to d). The bony structures and those with absolute percentage volume differences $< 2.5\%$ were regarded as volume constants (Table 2).

Structures with DSC differences $< 2.5\%$ included the brainstem, eyes, mandibles, oral cavity, temporal lobes, GTVp, and CTV1, with DSCs > 0.85 throughout treatment, and were regarded as morphologically stable. DSC changes exceeding 2.5% were observed in other structures. Linear fitting analysis revealed a decreasing trend ($R^2 \geq 0.7$) in the parotid glands, submandibular glands, thyroid, spinal cord, and target volumes (excluding GTVp), which temporally correlated with their volumetric dynamic patterns (Fig. 2e and f). No significant trends in DSC changes were observed for the other OARs. Most of them presented DSC values < 0.7 , indicating poor repeatability (Table 2).

Dosimetric changes

Dosimetric parameters for target volumes and OARs across weeks 1–7 were summarized in Table 3. The V100% for PGTVp ranged from 98.93% to 99.47%, and the V95% for PTV1 remained at 100%. However, PTV2 exhibited progressive dose degradation: the V95% decreased from 98.57% at week 1 to 94.04% at week 3, with the V100% decreasing from over 95% at weeks 1–5 to below 94% at weeks 6–7. The most pronounced target volume underdosing was observed in PGTVns, where V100% fluctuated between 85.18% and 92.61%, peaking in week 1 and reaching nadirs in weeks 3 and 5.

Most OARs showed no specific trend in dosimetric changes. However, linear fitting models revealed significant linear trends ($R^2 > 0.7$) in specific parameters (Fig. 3): Dmean to the parotid glands (+2.45 Gy cumulative increase, 31.80 Gy to 33.25 Gy), thyroid (+1.18 Gy, 45.40 Gy to 46.58 Gy), lenses, Dmax to the spinal cord, and D1% to the brainstem. Overall, all OARs maintained dose fluctuations within 3 Gy. The most significant dosimetric fluctuations in the structures with linear changes

occurred during weeks 3–6. During this period, the parameter changes for the parotid glands, thyroid, spinal cord, brainstem, and PTV2 were 1.77 Gy, 0.63 Gy, 0.76 Gy, 0.41 Gy, and 1.45%, respectively.

Discussion

In this study, 687 sets of FBCT scans were obtained for the 23 patients, with the interval between scans not exceeding two radiotherapy fractions. Therefore, the FBCT scans were uniformly distributed and effectively captured the weekly anatomical and dosimetric variations. Our findings revealed that during NPC radiotherapy, the morphology and dosimetry of the parotid glands, thyroid and CTV2 exhibited linear changes. Despite maintaining stable volumes, the brainstem and spinal cord showed an increasing trend in dose. Overall, the fluctuations in parameters for all OARs remained < 3 Gy, and the variations in target coverage remained within 10%. The most significant morphological and dosimetric changes were observed during weeks 3–6.

Historically, radiotherapy has relied mainly on repeat simulation scans or CBCT-based evaluations to monitor morphological and dosimetric changes, yet both methods present challenges: repeat simulation scans are time-consuming, and autosegmentation in CBCT images is hindered by severe artifacts, low soft-tissue contrast, and image truncations [19]. In our study, we employed low-dose FBCT scans (integrated within the linear accelerator) to perform prefraction imaging, reducing patient time and compliance burden. Moreover, compared with CBCT, FBCT offers superior soft-tissue resolution, enabling more precise automatic delineation of target volumes and OARs.

To improve the accuracy of automatic delineation, we developed specialized algorithms for GTVp, GTVns, CTVs, and OARs, each tailored to the distinct resolutions on FBCT and the anatomical relationships between target volumes and OARs. This approach offered several advantages: first, referencing the initial treatment planning contours helped minimize the risk of omitting GTVs; second, implementing critical OAR avoidance strategies during CTV delineation better aligned with established manual practices; and third, integrating additional convolutional layers into our volume-adapted 3D U-net further refined the segmentation of small OARs, enabling the DSC for small OARs such as the cochlea and IACs to exceed 0.75 [18]. Although this approach has enhanced research efficiency and study reliability, occasional under- or mis-segmentation still necessitated manual review.

Compared with previous studies that focused primarily on volume changes in the parotid gland and target volumes [1, 20], this study examined all OARs and target volumes in the NPC. However, only the parotid

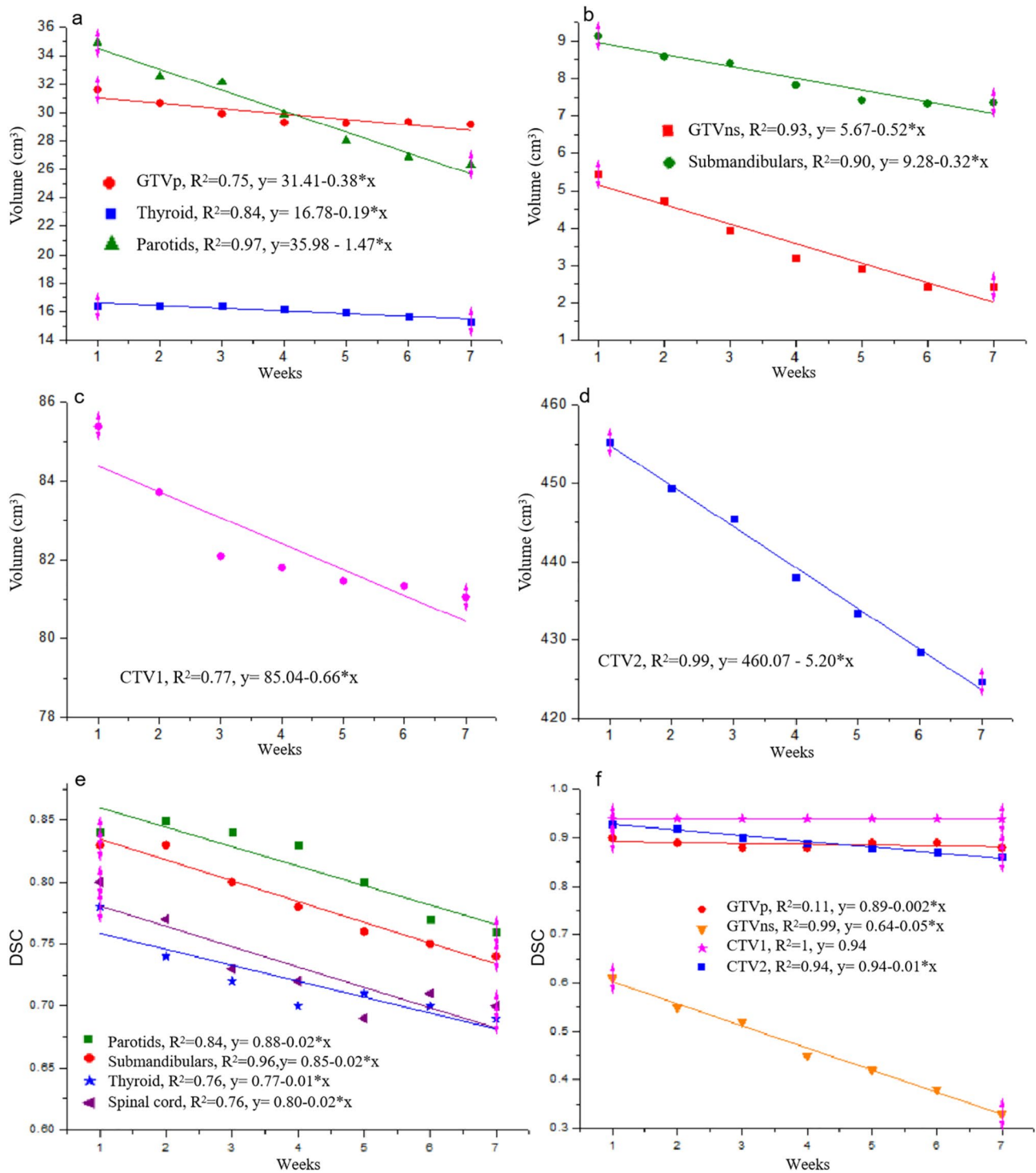


Fig. 2 Volumes and DSC linear changes for OARs and target volumes

glands, submandibular glands, thyroid and target volumes exhibited a linear decreasing trend. The parotid glands, submandibular glands and GTVns presented the most significant volume reductions, exceeding 20%. This finding aligned with previous studies reporting a 38.4% reduction in the GTV and a 15–35% decrease

in the parotid and submandibular glands [2, 21–24]. Unexpectedly, the structures with a linear decline in the DSC closely matched those with linear volume reductions, whereas not all the structures exhibited a gradual decrease in the DSC. This finding suggested that during

Table 2 The weekly volume and DSC of OARs and target volumes for 23 NPC patients included in this study

Structures	Week 1 (cm ³)	Week 2 (cm ³)	Week 3 (cm ³)	Week 4 (cm ³)	Week 5 (cm ³)	Week 6 (cm ³)	Week 7 (cm ³)	Average (cm ³)	Range of fluctuation (cm ³ , %)
Volume (cm ³)									
GTVp	31.60	30.67	29.93	29.30	29.25	29.35	29.17	29.90	-0.73 ~ 1.77 (-2.44 ~ 5.69)
GTVns	5.44	4.81	4.14	3.21	2.91	2.38	2.24	3.59	-1.35 ~ 1.85 (-37.60 ~ 51.53)
CTV1	85.40	83.72	82.09	81.81	81.47	81.34	81.06	82.41	-1.35 ~ 2.99 (-1.63 ~ 3.63)
CTV2	455.01	445.48	445.97	439.17	433.42	428.45	424.68	438.88	-14.20 ~ 16.13 (-3.24 ~ 3.68)
Parotids	34.90	32.55	32.13	29.89	28.00	26.87	26.33	31.10	-3.77 ~ 4.80 (-12.52 ~ 15.95)
Submandibulars	9.14	8.59	8.41	7.83	7.42	7.33	7.36	8.01	-0.68 ~ 1.14 (-8.49 ~ 14.11)
Thyroid	16.37	16.42	16.37	16.20	15.95	15.65	15.29	16.04	-0.75 ~ 0.38 (-4.68 ~ 2.37)
Larynx_Supraglottic	8.70	8.66	8.76	8.66	8.64	8.82	8.64	8.60	-0.06 ~ 0.06 (-0.69 ~ 0.69)
Larynx_Glotticx	5.62	5.69	5.63	5.69	5.73	5.64	5.69	5.67	-0.05 ~ 0.06 (-0.88 ~ 1.06)
OralCavity	196.19	195.97	195.85	196.58	194.65	196.16	196.56	195.99	-1.34 ~ 0.59 (-0.68 ~ 0.30)
Chiasm	0.76	0.76	0.74	0.75	0.74	0.76	0.76	0.75	-0.01 ~ 0.01 (-1.73 ~ 1.33)
OpticNerves	0.47	0.48	0.48	0.48	0.48	0.48	0.47	0.48	-0.01 ~ 0 (-2.08 ~ 0)
Lenses	0.20	0.21	0.20	0.20	0.20	0.20	0.20	0.20	0 (0)
Eyes	8.76	8.75	8.71	8.71	8.71	8.65	8.68	8.71	-0.06 ~ 0.04 (-0.69 ~ 0.46)
BraiStem	35.73	35.80	36.41	36.18	36.40	36.12	36.10	36.11	-1.37 ~ 0.47 (-1.05 ~ 0.83)
SpinalCord	21.52	21.03	20.94	21.24	21.34	21.47	21.44	21.28	-0.34 ~ 0.24 (-1.17 ~ 1.60)
TemporalLobes	113.93	113.28	113.02	114.76	114.85	114.46	114.14	113.78	-1.04 ~ 0.79 (-0.91 ~ 0.69)
Mandibles*	48.82	49.17	49.41	49.43	49.4	49.32	49.22	49.25	-
TMJs*	2.11	2.13	2.13	2.12	2.08	2.1	2.09	2.10	-
TympanicCavities*	0.57	0.56	0.56	0.55	0.55	0.56	0.55	0.56	-
Cochleas*	0.04	0.04	0.04	0.04	0.04	0.04	0.04	0.04	-
ETs*	0.15	0.16	0.16	0.14	0.15	0.15	0.15	0.15	-
Pituitary*	0.18	0.17	0.17	0.17	0.16	0.16	0.17	0.17	-
IACs*	0.10	0.10	0.11	0.10	0.09	0.10	0.10	0.10	-
Vestibul semises*	0.26	0.26	0.25	0.25	0.26	0.25	0.25	0.25	-
DSC									
GTVp	0.90	0.89	0.88	0.88	0.89	0.89	0.88	0.89	-0.01 ~ 0.001 (-1.12 ~ 1.12)
GTVns	0.61	0.55	0.52	0.45	0.42	0.38	0.33	0.47	-0.14 ~ 0.014 (-29.79 ~ 29.79)
CTV1	0.94	0.94	0.94	0.94	0.94	0.94	0.94	0.94	0 (0)
CTV2	0.93	0.92	0.90	0.89	0.88	0.87	0.86	0.89	-0.03 ~ 0.04 (-3.37 ~ 4.49)
Parotids	0.84	0.85	0.84	0.83	0.8	0.77	0.76	0.81	-0.05 ~ 0.004 (-6.17 ~ 4.94)
Submandibulars	0.83	0.83	0.8	0.78	0.76	0.75	0.74	0.78	-0.04 ~ 0.005 (-5.13 ~ 6.41)
Thyroid	0.78	0.74	0.72	0.70	0.71	0.70	0.69	0.72	-0.03 ~ 0.006 (-4.17 ~ 8.38)
Larynx_Supraglottic	0.46	0.41	0.44	0.40	0.45	0.43	0.41	0.43	-0.03 ~ 0.03 (-6.98 ~ 6.98)
Larynx_Glotticx	0.78	0.69	0.62	0.63	0.62	0.62	0.63	0.66	-0.04 ~ 0.012 (-6.06 ~ 18.18)
OralCavity	0.92	0.92	0.92	0.92	0.92	0.92	0.92	0.92	0 (0)
Chiasm	0.55	0.58	0.61	0.55	0.59	0.53	0.54	0.56	-0.03 ~ 0.05 (-5.36 ~ 8.93)
OpticNerves	0.58	0.57	0.56	0.56	0.56	0.57	0.53	0.56	-0.03 ~ 0.002 (-5.36 ~ 3.67)
Lenses	0.61	0.61	0.6	0.58	0.57	0.57	0.52	0.58	-0.06 ~ 0.03 (-10.34 ~ 5.17)
Eyes	0.89	0.89	0.89	0.89	0.88	0.88	0.87	0.88	-0.01 ~ 0.01 (-1.14 ~ 1.14)
BraiStem	0.88	0.89	0.89	0.89	0.88	0.88	0.88	0.88	0 ~ 0.01 (0 ~ 1.14)
SpinalCord	0.80	0.77	0.73	0.72	0.69	0.71	0.70	0.73	-0.04 ~ 0.007 (-5.48 ~ 9.59)
TemporalLobes	0.91	0.91	0.92	0.9	0.91	0.9	0.9	0.91	-0.01 ~ 0.001 (-1.11 ~ 1.11)
Mandibles	0.86	0.86	0.86	0.86	0.86	0.84	0.85	0.86	-0.02 ~ 0 (-2.33 ~ 0)
TMJs	0.51	0.5	0.52	0.49	0.51	0.49	0.48	0.50	-0.02 ~ 0.002 (-4.00 ~ 4.00)
TympanicCavities	0.81	0.79	0.74	0.79	0.79	0.78	0.77	0.78	-0.04 ~ 0.003 (-5.13 ~ 3.85)
Cochleas	0.50	0.50	0.55	0.50	0.54	0.48	0.49	0.51	-0.03 ~ 0.004 (-5.88 ~ 7.84)
ETs	0.63	0.64	0.61	0.59	0.63	0.61	0.58	0.61	-0.03 ~ 0.003 (-4.92 ~ 4.92)
Pituitary	0.61	0.57	0.68	0.65	0.61	0.61	0.61	0.62	-0.05 ~ 0.006 (-20.00 ~ 18.00)

Table 2 (continued)

Structures	Week 1 (cm ³)	Week 2 (cm ³)	Week 3 (cm ³)	Week 4 (cm ³)	Week 5 (cm ³)	Week 6 (cm ³)	Week 7 (cm ³)	Average (cm ³)	Range of fluctuation (cm ³ , %)
IACs	0.59	0.50	0.52	0.50	0.55	0.44	0.40	0.50	-0.1 ~ 0 0.09 (-4.92 ~ 4.92)
Vestibul semises	0.61	0.60	0.63	0.59	0.61	0.60	0.53	0.60	-0.07 ~ 0 0.03 (-11.67 ~ 5.00)

Abbreviations: NPC=Nasopharyngeal carcinoma; DSC=Dice similarity coefficient; OARs=Organs at risk; ET=Eustachian tube; IAC=Internal auditory canal; TMJ=Temporomandibular joint; GTVp=the gross target volume of primary tumor; GTVn=the gross tumor volume of lymph node; CTV=clinical target volume

* Bone structures, volume for display only, not included in analysis of volume change trend

Table 3 The weekly dosimetric parameter value of the OARs and target volumes

Structures	Week 1	Week 2	Week 3	Week 4	Week 5	Week 6	Week 7
PGTVp (V _{100%} [*] , %)	98.97	99.29	99.34	99.47	99.33	99.04	98.93
PGTVns (V _{100%} [*] , %)	92.61	89.22	87.46	90.39	85.46	90.4	91.44
PTV1 (V _{95%} [*] , %)	100.00	100.00	100.00	100.00	100.00	100.00	100.00
PTV2 (V _{95%} [*] , %)	98.57	98.22	98.14	94.04	97.86	96.98	97.51
PTV2(V _{100%} [*] , %)	96.22	95.26	95.23	95.39	95.11	93.78	93.21
Parotids (Dmean [#] , cGy)	3180.36	3236.08	3237.04	3280.34	3335.05	3414.11	3424.68
Submandibulars (Dmean [#] , cGy)	4880.87	4799.34	4790.62	4805.35	4847.51	4801.95	4821.98
Thyroid (Dmean [#] , cGy)	4540.17	4531.57	4540.21	4559.86	4604.27	4603.20	4658.08
Larynx_Supraglottic (Dmean [#] , cGy)	3567.32	3513.35	3535.27	3549.55	3566.38	3512.18	3520.60
Larynx_Glottis (Dmean [#] , cGy)	3628.75	3650.51	3674.69	3656.77	3662.75	3663.70	3660.65
OralCavity (Dmean [#] , cGy)	2955.84	2908.92	2910.03	2923.29	2912.60	2894.99	2910.32
Chiasm (Dmax ^{&} , cGy)	2229.40	2388.94	2370.06	2341.46	2309.34	2318.18	2184.63
OpticNerves (Dmax ^{&} , cGy)	2005.1	2143.86	2075.8	2161.02	2022.71	2006.58	1876.68
Lenses (Dmean [#] , cGy)	346.76	345.85	352.20	354.32	361.80	362.07	366.38
Eyes (Dmean [#] , cGy)	406.52	399.44	390.52	389.01	391.41	383.6	391.68
BrainStem (D1% [§] , cGy)	4877.78	4874.60	4888.94	4915.40	4919.90	4929.81	4915.25
SpinalCord (Dmax ^{&} , cGy)	3168.94	3166.33	3194.58	3233.88	3257.05	3270.47	3277.56
TemporalLobes (D1% [§] , cGy)	5223.10	5170.14	5184.49	5181.93	5182.63	5122.57	5098.57
Mandibles (D0.03cc [§] , cGy)	6333.18	6289.09	6307.64	6257.3	6258.68	6185.95	6171.82
TMJs (Dmax ^{&} , cGy)	4759.68	4734.09	4792.09	4761.71	4761.07	4794.59	4749.95
TympanicCavities (Dmean [#] , cGy)	3854.2	3890.47	3923.5	3867.13	3851.32	3856.82	3875.27
Cochleas (Dmean [#] , cGy)	4162.92	4127.96	4126.94	4096.26	4077.05	4073.23	4157.33
ETs (Dmean [#] , cGy)	5274.05	5263.76	5302.63	5290.22	5279.8	5240.47	5271.79
Pituitary (Dmean, cGy)	3536.13	3314.28	3330.95	3291.85	3322.07	3298.07	3380.71
IACs (Dmean [#] , cGy)	4094.28	4056.6	3962.44	3953.97	3927.79	3944.19	4011.22
Vestibul semises (Dmean [#] , cGy)	3602.01	3586.93	3632.93	3635.49	3614.32	3630.41	3629.32

Abbreviations: OARs=Organs at risk; ET=Eustachian tube; IAC=Internal auditory canal; TMJ=Temporomandibular joint; PGTVp=the planning gross target volume of primary tumor; PGTVn=the planning gross tumor volume of lymph node; PTV=planning target volume

* V100% and V95% of the target volumes means the coverage of 100% or 95% prescription dosage

The mean dose received by the organ

§ The minimum dose received by the "hottest" 1% or 0.03 cm³ of the organ

& The maximum dose received by the organ

NPC radiotherapy, volume changes can roughly reflect morphological changes.

Morphological variations during treatment induced dynamic dosimetric fluctuations. The V100% of PTV2 decreased from 96.22% at week 1 to 93.21% at week 7, indicating a linear reduction. Similarly, the V100% of PGTVns decreased by 7% from weeks 1–4, followed by a transient increase from weeks 6–7 (Table 3; Fig. 3), potentially attributable to late-phase lymph node shrinkage enhancing target coverage. Notably, the V100% of

PGTVp and the V95% of PTV1 remained relatively stable at approximately 99% and 100%, respectively, whereas Surucu et al. reported that the GTV coverage decreased from 99.3%–97.5% [3]. This discrepancy may stem from our GTVp referring to initial treatment planning contours, and only the anterior cavity was excluded, thereby minimizing anatomical alterations in GTVp and CTV1.

Progressive dose elevation was observed in the parotid glands, thyroid, brainstem, and spinal cord (Fig. 3). This finding aligned with established reports

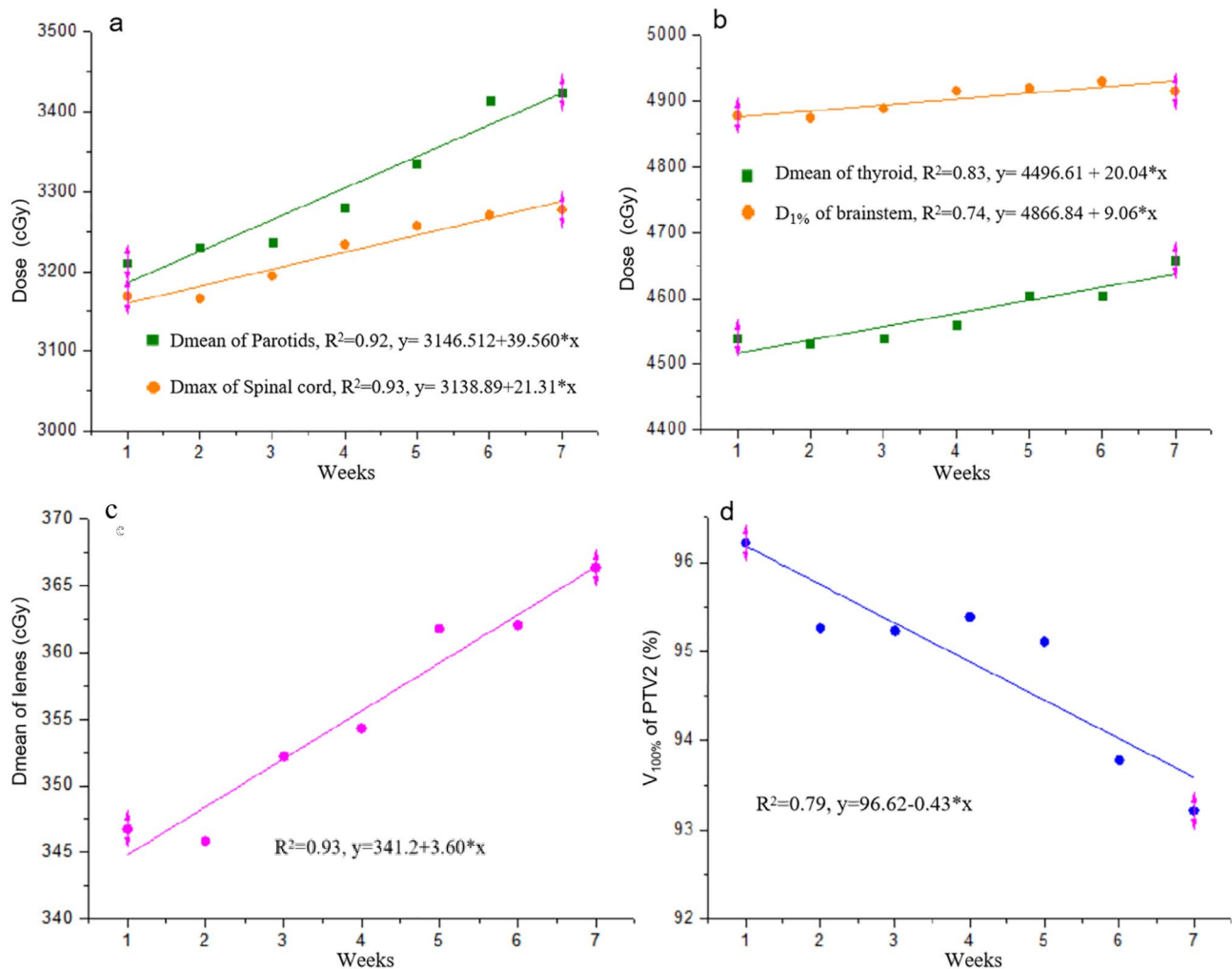


Fig. 3 Weekly dosimetric linear changes for OARs and target volumes

of cumulative dose escalation in the parotid gland, brainstem and spinal cord during head and neck tumor radiotherapy [3, 25], indicating that even morphologically stable structures may experience significant dosimetric drift due to subcutaneous fat reduction and superficial organ deformation. Notably, the gradual decline in target coverage and increased dose to OARs indicated that these changes were unrelated to positioning inaccuracy and could not be corrected by IGRT alone. This highlights the potential need for ART intervention. When making ART decisions, attention should be given to the morphological and dosimetric changes in the glandibular organs, brainstem, spinal cord and target volumes.

The peak dosimetric variations occurred during weeks 3–6, which aligned with findings from prior research [1, 4, 26]. During this period, deformation of the target volumes and OARs, along with dose variations, became more pronounced due to acute side effects such as pharyngeal pain and

xerostomia. Nevertheless, all OAR parameter fluctuations remained <3 Gy, and target coverage variations remained $\leq 10\%$ (Table 3). These findings suggested that frequent ART may not be necessary during NPC radiotherapy, with the optimal ART timing occurring at weeks 3–6. This finding was consistent with the proposals of Wu et al. and Gan et al. that two replans were sufficient for head-neck IMRT [6, 27].

Conclusions

In conclusion, progressive dosimetric deviations in OARs and targets during NPC radiotherapy cannot be addressed through IGRT alone, mandating the consideration of ART. Although morphological changes may approximate dose trends in the parotid glands, thyroid, and target volumes, stable OARs such as the spinal cord and brainstem paradoxically exhibit progressive dose accumulation, requiring vigilant dosimetric surveillance. The observed limited dose fluctuations (OARs <3 Gy, target coverage $<10\%$) support the

avoidance of frequent ART, with weeks 3–6 representing the optimal ART window.

Abbreviations

IMRT	Intensity-modulated radiation therapy
NPC	Nasopharyngeal carcinoma
OAR	Organs at risk
IGRT	Imaging-guided radiotherapy
ART	Adaptive radiotherapy
DSC	Dice similarity coefficient
GTV	Gross tumor volume
Dx% / Dy cc	The minimum dose received by the “hottest” x% or y cm ³ of the organ
FBCT	Fan beam computed tomography
PTV	Planning target volumes
TMJ	Temporomandibular joint
ET	Eustachian tubes
IAC	Internal auditory canals

Supplementary Information

The online version contains supplementary material available at <https://doi.org/10.1186/s13014-025-02643-6>.

Supplementary Material 1: Table S1. Multichannel grouping configuration for automated segmentation models of OARs.

Supplementary Material 2: Table S2. Voting results from the questionnaire on dosimetric parameters for target volume and OAR assessment.

Acknowledgements

Not applicable.

Author contributions

YX analyzed and interpreted the patient data, provided funding support, was a major contributor in writing the manuscript. HJ and YY collected patient information, organized and analyzed the data, and completed project administration. WG, YX, DW, LL (Lu Liu), JX and LL (Liu-wen Lin) collected and organized the FBCT images, morphological and dosimetric data. JL, LH and LY established the autosegmentation models, registered simulation CT scans with FBCT scans, recalculated treatment plans and extracted data on FBCT scans. SY and ZG proposed the concept, designed the article, provided funding support, and revised the manuscript. All authors read and approved the final manuscript.

Funding

This work was supported by grants from the Guangdong Basic and Applied Basic Research Foundation (No. 2024A1515030248), Fundamental Research Funds for the Central Universities, Sun Yat-sen University Clinical Research 5010 Program (No. 2024001) and Medical Scientific Research Foundation of Guangdong Province, China (No. A2024509).

Data availability

The datasets used and/or analysed during the current study are available from the corresponding author on reasonable request.

Declarations

Ethics approval and consent to participate

This retrospective study was approved by the local ethics committee of the institute [B2024-530-01], and the requirement for obtaining informed consent was waived.

Consent for publication

Not applicable.

Competing interests

The authors declare no competing interests.

Author details

¹Department of Radiation Oncology, Sun Yat-Sen University Cancer Center and State Key Laboratory of Oncology in Southern China, Collaborative Innovation Center of Cancer Medicine, 651 Dongfeng Road East, Guangzhou 510060, China

²Department of Radiation Oncology, Sun Yat-sen Memorial Hospital, Sun Yat-sen University and Guangdong Provincial Key Laboratory of Malignant Tumor Epigenetics and Gene Regulation, Guangzhou 510120, China

³Research Cooperation Department, Shenzhen United Imaging Research Institute of Innovative Medical Equipment, Shenzhen 518048, China

Received: 9 March 2025 / Accepted: 18 April 2025

Published online: 30 April 2025

References

- Wang H, Xue J, Ting Chen T, Qu T, Barbee D, Tam M, et al. Adaptive radiotherapy based on statistical process control for oropharyngeal cancer. *J Appl Clin Med Phys*. 2020;21:171–7. <https://doi.org/10.1002/acm2.12993>.
- Yan D, Lockman D, Martinez A, Wong J, Brabbins D, Vicini F, et al. Computed tomography guided management of interfractional patient variation. *Semin Radiat Oncol*. 2005;15:168–79. <https://doi.org/10.1016/j.semradonc.2005.01.07>.
- Surucu M, Shah KK, John C, Roeske JC, Choi M, Small W, Emami B. Adaptive radiotherapy for head and neck cancer. *Technol Cancer Res Treat*. 2017;16:218–23. <https://doi.org/10.1177/1533034616662165>.
- Bak B, Skrobala A, Adamska A, Malicki J. What information can we gain from performing adaptive radiotherapy of head and neck cancer patients from the past 10 years? *Cancer Radiother*. 2022;26:502–16. <https://doi.org/10.1016/j.canrad.2021.08.019>.
- Lemus OMD, Cao M, Cai B, Cummings M, Zheng D. Adaptive radiotherapy: Next-Generation radiotherapy. *Cancers (Basel)*. 2024;16:1206. <https://doi.org/10.3390/cancers16061206>.
- Gan Y, Langendijk JA, Oldehinkel E, Lin Z, Both S, Brouwer CL. Optimal timing of replanning for head and neck adaptive radiotherapy. *Radiother Oncol*. 2024;194:110145. <https://doi.org/10.1016/j.radonc.2024.110145>.
- Castelli J, Thariat J, Benezery K, Hasbini A, Gery B, Berger A, et al. Weekly adaptive radiotherapy vs standard Intensity-Modulated radiotherapy for improving salivary function in patients with head and neck cancer: A phase 3 randomized clinical trial. *JAMA Oncol*. 2023;9:1056–64. <https://doi.org/10.1001/jamaoncol.2023.1352>.
- Schwartz DL. Current progress in adaptive radiation therapy for head and neck cancer. *Curr Oncol Rep*. 2012;14:139–47. <https://doi.org/10.1007/s11912-012-0221-4>.
- Yan D. Adaptive radiotherapy: merging principle into clinical practice. *Semin Radiat Oncol*. 2010;20:79–83. <https://doi.org/10.1016/j.semradonc.2009.11.001>.
- Brouwer CL, Steenbakkers RJHM, Langendijk JA, Sijtsema NM. Identifying patients who may benefit from adaptive radiotherapy: does the literature on anatomic and dosimetric changes in head and neck organs at risk during radiotherapy provide information to help? *Radiother Oncol*. 2015;115:285–94. <https://doi.org/10.1016/j.radonc.2015.05.018>.
- Chatterjee S, Maulik S, Prasath S, Arun B, Das A, Chakrabarty S, et al. Xerostomia quality of life and resource requirements following Parotid sparing adaptive radiotherapy in head and neck cancers: results of a prospective cohort study (Study ID CTRI/2017/11/010683). *Radiother Oncol*. 2022;168:250–5. <https://doi.org/10.1016/j.radonc.2022.01.020>.
- Bhide SA, Davies M, Burke K, McNair HA, Hansen V, Barbachano Y, et al. Weekly volume and dosimetric changes during chemoradiotherapy with intensity-modulated radiation therapy for head and neck cancer: a prospective observational study. *Int J Radiat Oncol Biol Phys*. 2010;76:1360–8. <https://doi.org/10.1016/j.ijrobp.2009.04.005>.
- Zhao L, Wan Q, Zhou Y, Deng X, Xie C, Wu S. The role of replanning in fractionated intensity modulated radiotherapy for nasopharyngeal carcinoma. *Radiother Oncol*. 2011;98:23–7. <https://doi.org/10.1016/j.radonc.2010.10.009>.
- Hansen EK, Bucci MK, Quivey JM, Weinberg V, Xia P. Repeat CT imaging and replanning during the course of IMRT for head-and-neck cancer. *Int J Radiat Oncol Biol Phys*. 2006;64:355–62. <https://doi.org/10.1016/j.ijrobp.2005.07.957>.
- Langendijk JA, Doornaert P, Verdonck-de Leeuw IM, Leemans CR, Aaronson NK, Slotman BJ. Impact of late treatment-related toxicity on quality of life

- among patients with head and neck cancer treated with radiotherapy. *J Clin Oncol.* 2008;26:3770–6. <https://doi.org/10.1200/JCO.2007.14.6647>.
16. Belshaw L, Agnew CE, Irvine DM, Rooney KP, McGarry CK. Adaptive radiotherapy for head and neck cancer reduces the requirement for rescans during treatment due to spinal cord dose. *Radiat Oncol.* 2019;14:189. <https://doi.org/10.1186/s13014-019-1400-3>.
 17. Yu L, Zhao J, Zhang Z, Wang J, Hu W. Commissioning of and preliminary experience with a new fully integrated computed tomography Linac. *J Appl Clin Med Phys.* 2021;22:208–23. <https://doi.org/10.1002/acm2.13313>.
 18. Yang YX, Yang X, Jiang XB, Lin L, Wang GY, Sun WZ, et al. Artificial Intelligence-Empowered multistep integrated radiation therapy workflow for nasopharyngeal carcinoma. *Int J Radiat Oncol Biol Phys.* 2024;19(S0360–30162403670–8). <https://doi.org/10.1016/j.ijrobp.2024.11.096>.
 19. Glide-Hurst CK, Lee P, Yock AD, Olsen JR, Cao M, Siddiqui F, et al. Adaptive radiation therapy (ART) strategies and technical considerations: A state of the ART review from NRG oncology. *Int J Radiat Oncol Biol Phys.* 2021;109:1054–75. <https://doi.org/10.1016/j.ijrobp.2020.10.021>.
 20. Castelli J, Simon A, Louvel G, Henry O, Chajon E, Nassef M, et al. Impact of head and neck cancer adaptive radiotherapy to spare the Parotid glands and decrease the risk of Xerostomia. *Radiat Oncol.* 2015;10:6. <https://doi.org/10.1186/s13014-014-0318-z>.
 21. Yao WR, Xu SP, Liu B, Cao XT, Ren G, Du L, et al. Replanning criteria and timing definition for parotid protection-based adaptive radiation therapy in nasopharyngeal carcinoma. *Biomed Res Int.* 2015;2015:476383. <https://doi.org/10.1155/2015/476383>.
 22. Castadot P, Geets X, Lee JA, Christian N, Grégoire V. Assessment by a deformable registration method of the volumetric and positional changes of target volumes and organs at risk in pharyngo-laryngeal tumors treated with concomitant chemoradiation. *Radiat Oncol.* 2010;95:209–17. <https://doi.org/10.1016/j.radonc.2010.03.007>.
 23. Vásquez Osorio EM, Hoogeman MS, Al-Mamgani A, Teguh DN, Levendag PC, Heijmen BJM. Local anatomic changes in Parotid and submandibular glands during radiotherapy for oropharynx cancer and correlation with dose, studied in detail with nonrigid registration. *Int J Radiat Oncol Biol Phys.* 2008;70:875–82. <https://doi.org/10.1016/j.ijrobp.2007.10.063>.
 24. Wang Z-H, Yan C, Zhang Z-Y, Zhang CP, Hu HS, Kirwan J, et al. Radiation-induced volume changes in Parotid and submandibular glands in patients with head and neck cancer receiving postoperative radiotherapy: a longitudinal study. *Laryngoscope.* 2009;119:1966–74. <https://doi.org/10.1002/lary.20601>.
 25. Franzese C, Tomatis S, Bianchi SP, Pelizzoli M, Teriaca MA, Badalamenti M, et al. Adaptive Volumetric-Modulated Arc radiation therapy for head and neck cancer: evaluation of benefit on target coverage and sparing of organs at risk. *Curr Oncol.* 2023;30:3344–54. <https://doi.org/10.3390/curroncol30030254>.
 26. Bhandari V, Patel P, Gurjar OP, Gupta KL. Impact of repeat computerized tomography Replans in the radiation therapy of head and neck cancers. *J Med Phys.* 2014;39:164–8. <https://doi.org/10.4103/0971-6203.139005>.
 27. Wu Q, Chi Y, Chen PY, Krauss DJ, Yan D, Martinez A. Adaptive replanning strategies accounting for shrinkage in head and neck IMRT. *Int J Radiat Oncol Biol Phys.* 2009;75:924–32. <https://doi.org/10.1016/j.ijrobp.2009.04.047>.

Publisher's note

Springer Nature remains neutral with regard to jurisdictional claims in published maps and institutional affiliations.